Journal of Power Sources 196 (2011) 6768–6771

Contents lists available at ScienceDirect

Journal of Power Sources

journal homepage: www.elsevier.com/locate/jpowsour

The electrochemical behavior of low-temperature synthesized $FeSn_2$ nanoparticles as anode materials for Li-ion batteries

U.G. Nwokeke [a], R. Alcántara [a], J.L. Tirado [b,*], R. Stoyanova [b], E. Zhecheva [b]

[a] Laboratorio de Química Inorgánica, Universidad de Córdoba, 14071 Córdoba, Spain
[b] Institute of General and Inorganic Chemistry, Bulgarian Academy of Sciences, 1113 Sofia, Bulgaria

ARTICLE INFO

Article history:
Received 13 July 2010
Received in revised form
20 September 2010
Accepted 25 October 2010
Available online 3 November 2010

Keywords:
Lithium-ion batteries
Iron/tin intermetallics
Mössbauer spectroscopy
Electron paramagnetic resonance

ABSTRACT

Tin-containing nanometric and amorphous intermetallics and alloys are envisaged as negative electrodes for high-capacity lithium ion batteries. Nanocrystalline $FeSn_2$ has been prepared by reduction of Sn^{2+} and Fe^{3+} in tetraethylene glycol at 185 °C. Microcrystalline $FeSn_2$ has been prepared at 490 °C. The properties of nano-$FeSn_2$ and micro-$FeSn_2$ have been observed to be very different. The small particles size hinders the long-range magnetism and consequently the Mössbauer spectra are modified. The nanocrystalline particles of $FeSn_2$ show exothermal effects in the DTA experiment that are not observed in the micrometric particles. Nanocrystalline $FeSn_2$ exhibits a much better electrochemical behavior and electrode stability than microcrystalline $FeSn_2$.

1. Introduction

Several tin compounds and alloys are very attractive for the replacement of graphite in lithium-ion batteries. Thus, tin can alloy with lithium up to the composition $Li_{4.4}Sn$ (equivalent to 990 mAh g^{-1}). The 3*d* elements and tin form many intermetallic compounds, such as $CoSn_2$, $FeSn_2$, CoSn, Cu_6Sn_5, $CoSn_3$ and Ti_2Sn_3. Several of these intermetallics can be useful as electrode active materials and exhibit better stability than pure tin. The intermetallic compound $FeSn_2$ was early considered as a potential candidate for the negative electrode of Li-ion batteries [1]. As compared with the isostructural $CoSn_2$ compound (space group *I*4/*mcm*), the use $FeSn_2$ may have positive economic and environmental effects.

The intermetallics with very small particles size can exhibit modified properties in comparison with bulk materials. The small particle sizes of the intermetallic compounds can be advantageous for their use in lithium ion batteries electrodes. The nanometric particles have low diffusion path lengths and can exhibit better ability to buffer the lattice volume changes due to the lithium uptake.

In order to evaluate the effect of particle size on the properties and electrochemical performance of $FeSn_2$, we have synthesized nanocrystalline intermetallic powders of $FeSn_2$ from metal salt precursors via chemical reduction in tetraethylene glycol at relatively low temperature [2]. In Ref. [2] only a nano material was studied. In this work, we have extended the study by reporting new data and comparing between micro and nano, which unfolds the origin of the better performance at the nano scale. The structural characterization was done by powder XRD and transmission electron microscopy (TEM). The electrochemical behavior and reaction mechanism of the $FeSn_2$ nanocrystals were investigated by XRD, Mössbauer spectroscopy (MS) and electron paramagnetic resonance (EPR) spectroscopy. The goal of this work is to study the differences between the properties of nano-$FeSn_2$ and micro-$FeSn_2$ and their influence on the electrochemical behavior.

2. Experimental

Microcrystalline $FeSn_2$ was prepared by heating a stoichiometric mixture of Sn and Fe powders under Ar atmosphere at 490 °C during 10 h. This sample is referred to as micro-$FeSn_2$.

Nanocrystalline $FeSn_2$ was prepared at 185 °C using a one-pot method based on the reduction of ions in tetraethylene glycol (TEG) as was previously reported elsewhere [2]. $SnCl_2$ and $FeCl_3{\cdot}6H_2O$ were used as sources of the metals. $NaBH_4$ was used to reduce the ions. The organic polymers PVP and PEO were used to stabilize the metallic particles. Firstly, tin ions are reduced to form nanometric particles of metallic tin. Then, the iron ions are reduced and diffuse into the tin particles. This sample is referred to as nano-$FeSn_2$.

The XRD patterns were obtained using a Siemens D500 instrument equipped with CuKα radiation. TEM and SEM images were

* Corresponding author at: Laboratorio de Química Inorgánica, Universidad de Córdoba, Edificio C3, planta 1, Campus de Rabanales, 14071 Córdoba, Spain. Tel.: +34 957218637; fax: +34 957218621.
E-mail address: iq1ticoj@uco.es (J.L. Tirado).

0378-7753/$ – see front matter © 2010 Elsevier B.V. All rights reserved.
doi:10.1016/j.jpowsour.2010.10.071

recorded in a JEM-2010 and a JSM-6300 apparatus, respectively. The ^{57}Fe Mössbauer spectra were recorded in a Wissel instrument. An iron foil was used for the calibration of the Mössbauer spectroscopy instrument.

Differential thermal analysis (DTA) experiments were performed in a Shimadzu DTG-60 instrument, using alumina pans and a heating rate of 10 °C min^{-1}. A continuous Ar-flow of 70 mL min^{-1} was used as purging gas and to create an inert atmosphere. To remove the air, the Ar-flow was initiated 50 min prior to starting the DTA measurement. The employed Ar had 2 ppm of O_2 and 2 ppm of H_2O impurities. The continuous flow of Ar was electronically controlled with a Bronkhorst apparatus.

EPR spectra were registered at X-band (9.23 GHz) as the first derivative of the absorption signal using ERS 220/Q spectrometer in the temperature range 90–410 K. The *g*-factors were established with respect to a Mn^{2+}/ZnS standard. The signal intensity was determined by double integration of the experimental EPR spectrum. For EPR measurements of anode materials, the samples were manipulated in a glove box in Ar atmosphere.

The electrochemical experiments were carried out using lithium test cells in a MacPile instrument. The electrolyte solution was $LiPF_6$ salt dissolved in ethylene carbonate:diethyl carbonate solvent mixture. A piece of Li was used as negative electrode. The positive electrodes were constituted by $FeSn_2$ (active material, 77%), PVDF (binder agent, 8%) and graphite (conductive agent, 15%). Both iron and tin atom masses are used to compute the gravimetric capacities.

3. Results and discussion

The intermetallic compound $FeSn_2$ prepared by ions reduction in TEG at 185 °C is composed of nanosized particles of around 20 nm of diameter (Fig. 1a) and exhibits broadened XRD reflections. These nanoparticles tend to form aggregates. The sample prepared by heating powders of Fe and Sn at 490 °C under Ar atmosphere is composed of micrometric particles with irregular morphologies (Fig. 1b) and exhibits narrow XRD reflections. The EDAX microanalysis reveals that the experimental tin/iron ratio is the expected, for both micro-$FeSn_2$ and nano-$FeSn_2$ samples.

The ^{57}Fe MS of $FeSn_2$ are shown in Fig. 2. The spectra illustrate the influence of particle size on magnetic ordering. Micro-$FeSn_2$ shows a sextuplet at isomer shift value $\delta = 0.50(1)$ mm s^{-1} due to the expected antiferromagnetic behavior. In contrast, the ^{57}Fe MS of the nano-$FeSn_2$ sample shown in Fig. 1 contains a singlet signal at isomer shift value $\delta = 0.51(4)$ mm s^{-1}, which is indicative of a superparamagnetic state at room temperature. The small particle size hinders the long-range magnetism. The particles with very small size can exhibit smaller recoil-free fraction and drive to MS with lower intensity and broadened [3].

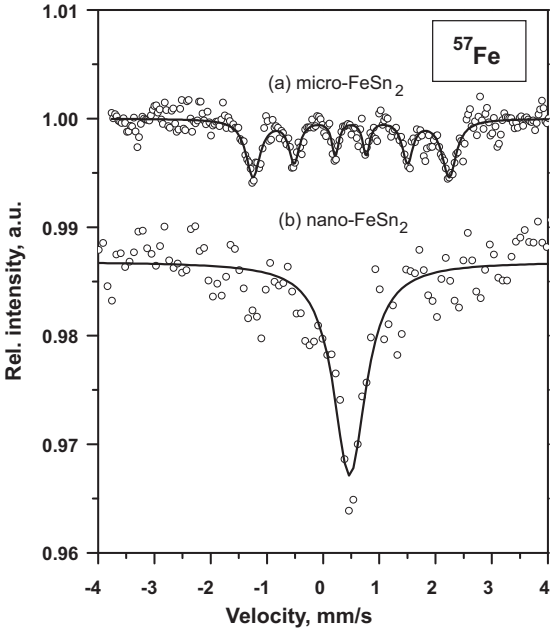

Fig. 2. Room temperature ^{57}Fe Mössbauer spectra for (a) micro-$FeSn_2$ and (b) nano-$FeSn_2$.

The EPR results are in agreement with the magnetic properties and MS. The EPR spectrum of pristine nano-$FeSn_2$ consists of a nearly symmetric line (Fig. 3). On cooling, the EPR signal becomes anisotropic. At the same time, the EPR signal intensity decreases and, below 140 K, the signal disappears. This is consistent with our previous studies on the formation of nanocrystalline $FeSn_2$ [2]. Therefore, the EPR signal of nano-$FeSn_2$ can be assigned to magnetically correlated spins, which are ordered in a long-range below 140 K.

Differential thermal analysis results for micro- and nano-$FeSn_2$ are shown in Fig. 4. Firstly, the DTA curve was obtained while heating the sample under Ar-flow. Then, the sample was cooled with continuous Ar-flow, and the second DTA curve was obtained by reheating under Ar-flow. After cooling under Ar-flow, the inert gas flow was stopped and the third DTA curve was obtained by reheating the sample in air. The first heating process of nano-$FeSn_2$ under Ar-flow shows a broad exothermal feature between ca. 200 and 430 °C, while no endothermal peak is observed at the melting point of pure tin (232 °C). This exothermal region has a complex

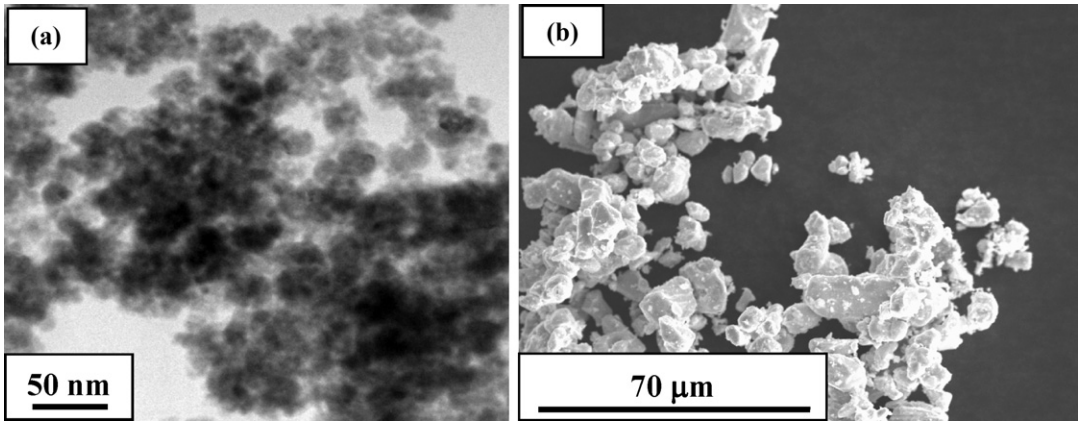

Fig. 1. (a) TEM image of nano-$FeSn_2$ and (b) SEM image of micro-$FeSn_2$.

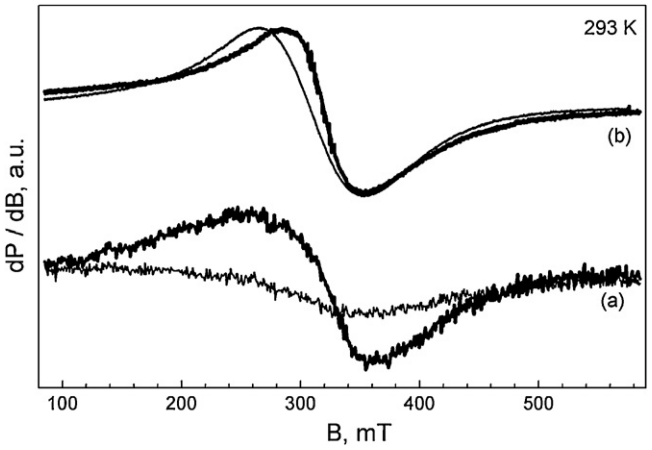

Fig. 3. EPR spectra of pristine $FeSn_2$ (a) and $FeSn_2$ discharged up to 1.15 V (b) registered at 293 K (bold lines) and 143 K (thin lines).

nature and may involve several processes. In principle, it may be related to the growth of the nanocrystalline grains and reduction of their surface energy, phase transformation and oxidation. Exothermal peaks were also previously reported for nano-$CoSn_3$ [4] and nano-$Sn_3Co_3C_4$ [5]. The participation of oxidative processes due to traces of oxygen cannot be ruled out, particularly due to the expected reactivity of the surface of very small metallic particles. For example, previous studies showed that metallic Fe nanoparticles are exothermally oxidized at 177 °C [6]. To ensure the validity of the results, after this first heating process, the same sample was cooled and re-heated under continuous Ar-flow. The second heating process shows no thermal events. On the contrary, the DTA curve of micro-$FeSn_2$ does not show any exothermal processes in the first heating from room temperature to 700 °C. Small endothermal peaks are observed at 443 °C and around 513–540 °C which more probably are related to phase transformations.

According to its phase diagram, $FeSn_2$ decomposes at 513 °C. In the second heating of micro-$FeSn_2$ (Fig. 4), an intense and endothermal peak is observed at the melting point of Sn, indicating the previous decomposition of micro-$FeSn_2$ during the first heating. Since the melting peak of Sn is not observed in the second heating of nano-$FeSn_2$, it can be deduced that nano-$FeSn_2$ does not decompose in the first heating most probably because it is oxidized with traces of oxygen. The third heating process (not shown) was carried

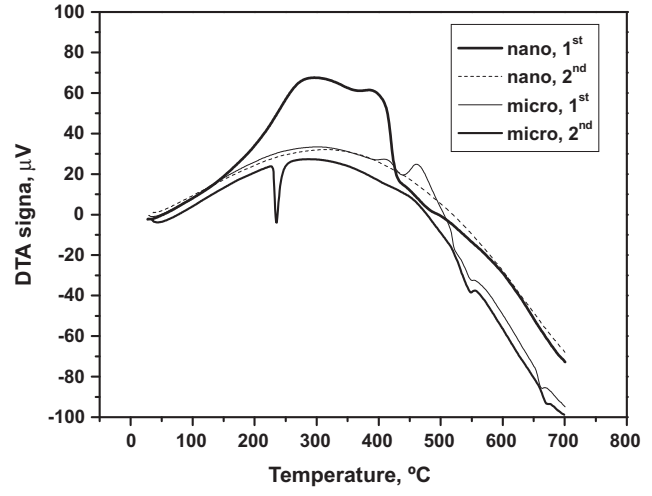

Fig. 4. DTA of nano- and micro-$FeSn_2$ for the first and second heating processes under Ar-flow.

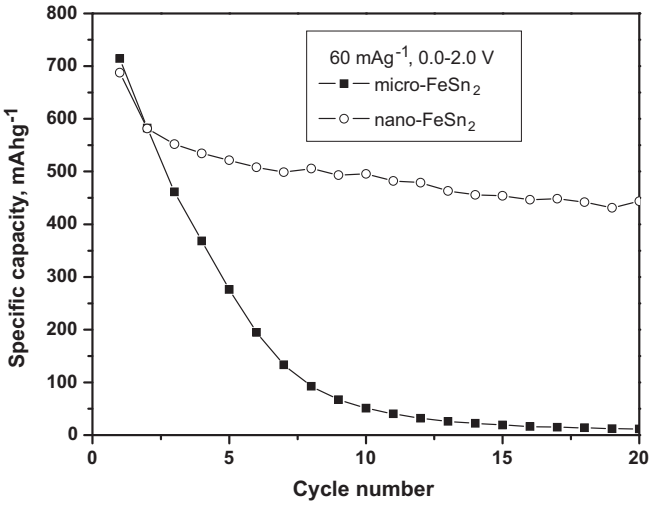

Fig. 5. Specific capacity as a function of cycle number for microcrystalline and nanocrystalline $FeSn_2$.

out in air, and no thermal events were observed for nano-$FeSn_2$. The XRD pattern (not shown) of the nanosized sample after the third heating showed only very broadened reflections corresponding to SnO_2. The third heating process of the microsized sample (in air) shows the endothermal peak of tin melting point and an exothermal peak at 484 °C as a result of oxidation in air. The XRD patterns of the sample recuperated from this last DTA experiment confirmed the occurrence of SnO_2 and Fe_2O_3. These results show the higher reactivity of the surface of the intermetallic nanoparticles in comparison with the microparticles.

The effect of the particle size is particularly dramatic in the electrochemical performance. Nano-$FeSn_2$ exhibits much better electrochemical behavior than micro-$FeSn_2$ (Figs. 5 and 6). A reversible discharge capacity above 500 mAh g^{-1} is observed in lithium test cells (Fig. 5). In comparison with bulk samples and results already in literature, there is a significant improvement in electrochemical behavior which makes it an interesting anode material for lithium-ion batteries. Two possibilities of poor capacity retention in microparticles: core not reached by lithium or particle fragmentation due to mechanical stresses leading to the loss of electrical contact. To discern between both options, it can be seen that both samples have almost the same capacity during the first two cycles. Thus the core of the particles seems to be accessible to lithium for the starting material in both samples.

The derivative plots of the corresponding galvanostatic discharge–charge cycles are shown in Fig. 6 for micro-$FeSn_2$ and nano-$FeSn_2$. The formation of surface films in the very small particles is more evident for the first discharge of nano-$FeSn_2$, and an irreversible peak is observed at 1.3 V. This result is in good agreement with the DTA experiments shown above that demonstrate a higher surface reactivity for nano-$FeSn_2$. The reduction of amorphous oxides in the surface of the nanoparticles also may contribute to the irreversible peak at 1.3 V. The higher surface reactivity is also demonstrated by the EPR spectrum of nano-$FeSn_2$ discharged up to 1.15 V. The EPR spectrum of pristine nano-$FeSn_2$ is changed at lower depth of discharge, as a result of which a single Lorentzian line becomes visible (Fig. 3b). The signal is broadened on cooling (from 300 to 100 K) together with a shift of the effective resonance absorption towards a lower magnetic field (Fig. 3b). Based on the EPR studies of charged and discharge $FeSn_2$ [2], the observed EPR parameters can be attributed to superparamagnetic iron particles.

The occurrence of Li_xSn phases is evidenced by several peaks in both micro- and nanosized samples. The peak at 0.58 V in the first charge of micro-$FeSn_2$, which corresponds to the extraction

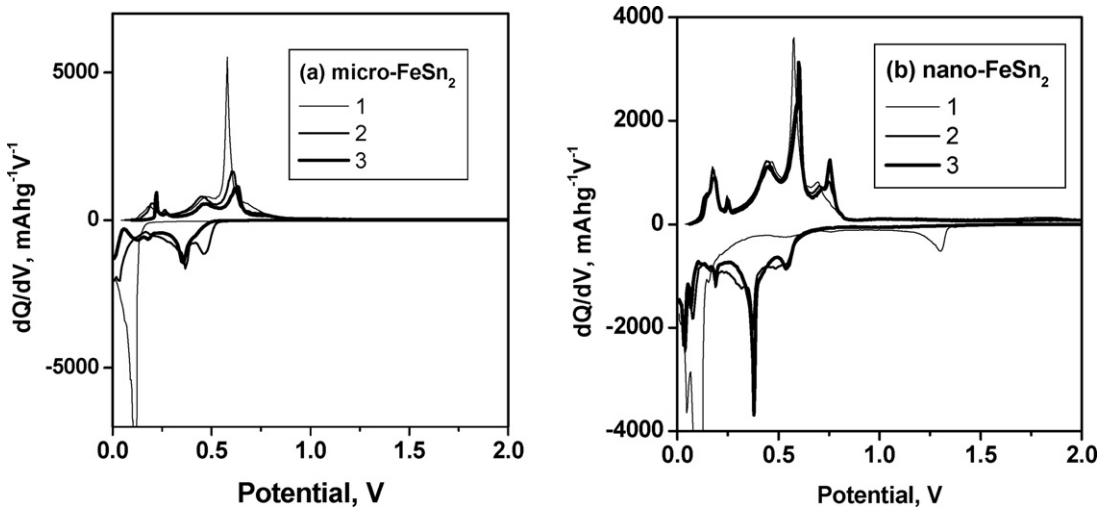

Fig. 6. Derivative plots of the first three cycles for (a) micro-$FeSn_2$ and (b) nano-$FeSn_2$.

of lithium from Li_xSn phases, becomes less intense and is shifted to higher potentials from the first to the third cycle. It seems that lithium is hardly removed from the Li_xSn grains. The peak at ca. 0.4 V in the discharge process shifts to lower potentials when the cycle number increases. Consequently, the polarization of the cell is higher for the micro-$FeSn_2$ when the cycle number increases. In contrast, the derivative plot of nano-$FeSn_2$ remains almost unchanged after the first discharge, suggesting the best stability of the electrode nanomaterial. The electrochemical process involves the conversion of the $FeSn_2$ nanocrystals into Li_xSn phases. Particles of super-paramagnetic Fe are also observed in the EPR spectra [2], indicating that the majority of the Fe atoms are not involved in the back reaction during charge after several cycles. The spectroscopy study reveals the formation of superparamagnetic tin-doped iron particles during cell discharge that are preserved during the recharge process, while a partial recovery of the $FeSn_2$ structure takes place [2]. The reaction mechanism of nano-$FeSn_2$ differs from micro-$FeSn_2$, which evidences the dramatic effect commonly exerted by nanodispersion on the behavior of electrode materials for lithium ion batteries. In the case of micro-$FeSn_2$, the iron particles do not hold the processes of alloying/dealloying between tin and lithium.

The origin of the better behavior of the nano-sample results from two different phenomena. First, both micro- and nano-particles seem to react completely with lithium during the first discharge, as evidenced by the initial capacities, which have similar values. However, capacity degrades sharply on successive cycles for the micro-sample. It is a well-known fact that tin intermetallics suffer giant volume changes on lithium insertion–deinsertion, which lead to particle fragmentation and the loss of electrical contacts, with the subsequent capacity fade [7–11]. This is avoided in the nano-sample, as the size of the particles is sufficiently low (as shown by both ^{57}Fe MS and EPR) to retain a small size basically unaltered during cycling. A second factor is the lack of participation of iron nanoparticles generated after the first discharge in the cycling of the nano-sample, which has been demonstrated above from EPR data. This phenomenon provides a constant conducting matrix of metallic particles which also contributes to the preservation of the size of the nanodomain.

4. Conclusions

Nanoparticles of crystalline $FeSn_2$ have been successfully prepared below 200 °C. The magnetic ordering in $FeSn_2$ is affected by the particle size. The nanoparticles of $FeSn_2$ are more reactive than the microparticles, as the DTA results have revealed. The obtained nano-$FeSn_2$ material exhibits a much better electrochemical behavior than micro-$FeSn_2$ obtained at 490 °C. The electrochemical behavior of micro-$FeSn_2$ deteriorates very rapidly in a few cycles. The nanoparticles of $FeSn_2$ form a stable electrode nanomaterial, while the electrode based on micro-$FeSn_2$ has very little stability. The superparamagnetic-Fe nanoparticles that are formed in the discharged electrode avoid the growth of the tin particles and improve the electrochemical performance.

Acknowledgments

R.A. acknowledges the financial support from MICNN (grant CTQ2008-03192/BQU). U.N. is indebted to ALISTORE-ERI. J.L.T. acknowledges the financial support from MICNN (grant MAT2008-05880). Authors are grateful to the financial support from the National Science Fund of Bulgaria (Contracts Ch 1701/2007 and DO-02-82/2008).

References

[1] O. Mao, R.D. Dunlap, J.R. Dahn, J. Electrochem. Soc. 146 (1999) 405.
[2] U.G. Nwokeke, R. Alcántara, J.L. Tirado, R. Stoyanova, M. Yoncheva, E. Zhecheva, Chem. Mater. 22 (2010) 2268.
[3] R. Alcántara, P. Lavela, G. Ortiz, I. Rodríguez, J.L. Tirado, Hyperfine Interact. 187 (2008) 13.
[4] R. Alcántara, U. Nwokeke, I. Rodríguez, J.L. Tirado, Electrochem. Solid-State Lett. 11 (2008) A209.
[5] J.S. Thorne, P.P. Ferguson, R.D. Dunlap, J.R. Dahn, J. Alloys Compd. 472 (2009) 390.
[6] X.G. Li, A. Chiba, S. Takahashi, K. Ohsaki, J. Magn. Magn. Mater. 173 (1997) 101.
[7] M. Winter, J.O. Besenhard, Electrochim. Acta 45 (1999) 31.
[8] L.Y. Beaulieu, K.W. Eberman, R.L. Turner, L.J. Krause, J.R. Dahn, Electrochem. Solid-State Lett. 4 (2001) A137.
[9] N. Li, C.R. Martin, B. Scrosati, J. Power Sources 97–98 (2002) 240.
[10] J.L. Tirado, Mater. Sci. Eng. R 40 (2003) 103.
[11] A.S. Aricò, P. Bruce, B. Scrosati, J.M. Tarascon, W. van Schalkwijk, Nat. Mater. 4 (2005) 366.